THE JOURNAL OF BIOLOGICAL CHEMISTRY VOL. 286, NO. 10, pp. 8176–8187, March 11, 2011

Residues 155 and 348 Contribute to the Determination of $P2X_7$ Receptor Function via Distinct Mechanisms Revealed by Single-nucleotide Polymorphisms*[S]

Received for publication, December 10, 2010 Published, JBC Papers in Press, January 4, 2011, DOI 10.1074/jbc.M110.211284

Helen J. Bradley[1], Jocelyn M. Baldwin[2], G. Ranjan Goli[2], Brian Johnson, Jie Zou, Asipu Sivaprasadarao, Stephen A. Baldwin, and Lin-Hua Jiang[3]

From the Institute of Membrane and Systems Biology, Faculty of Biological Sciences, University of Leeds, Leeds LS2 9JT, United Kingdom

$P2X_7$ receptors are important in mediating the physiological functions of extracellular ATP, and altered receptor expression and function have a causative role in the disease pathogenesis. Here, we investigated the mechanisms determining the $P2X_7$ receptor function by following two human single-nucleotide polymorphism (SNP) mutations that replace His-155 and Ala-348 in the human (h) $P2X_7$ receptor with the corresponding residues, Tyr-155 and Thr-348, in the rat (r) $P2X_7$ receptor. H155Y and A348T mutations in the $hP2X_7$ receptor increased ATP-induced currents, whereas the reciprocal mutations, Y155H and T348A, in the $rP2X_7$ receptor caused the opposite effects. Such a functional switch is a compelling indication that these residues are critical for $P2X_7$ receptor function. Additional mutations of His-155 and Ala-348 in the $hP2X_7$ receptor to residues with diverse side chains revealed a different dependence on the side chain properties, supporting the specificity of these two residues. Substitutions of the residues surrounding His-155 and Ala-348 in the $hP2X_7$ receptor with the equivalent ones in the $rP2X_7$ receptor also affected ATP-induced currents but were not fully reminiscent of the H155Y and A348T effects. Immunofluorescence imaging and biotin labeling assays showed that H155Y in the $hP2X_7$ receptor increased and Y155H in the $rP2X_7$ receptor decreased cell-surface expression. Such contrasting effects were not obvious with the reciprocal mutations of residue 348. Taken together, our results suggest that residues at positions 155 and 348 contribute to $P2X_7$ receptor function via determining the surface expression and the single-channel function, respectively. Such interpretations are consistent with the locations of the residues in the structural model of the $hP2X_7$ receptor.

$P2X_7$ receptors belong to the ionotropic purinergic P2X receptor family (1–5). The receptor expression is well documented in immune cells, glial cells in the brain, satellite cells in the peripheral nervous system, bone, and epithelial cells, where the receptor serves as the primary mediator for numerous physiological functions of extracellular ATP, including immune responses, inflammation, cell proliferation, neuron-glial cell interactions, nociception, bone remodeling, and saliva secretion (6–17). The receptor is thought to be a homotrimer (18) with three subunits intertwining together along a vertical ion-conducting pathway. Each subunit contains two transmembrane domains (TM1 and TM2) joined by a large ectodomain, and both N and C termini reside intracellularly. Functional characterizations of mammalian $P2X_7$ receptors have identified several distinguishing features, including activation by submillimolar concentrations of ATP and a higher sensitivity to benzoylbenzoyl-ATP (BzATP),[4] a synthetic ATP analog, than to ATP (19–21). In addition to operating as ATP-gated Ca^{2+}-permeable cation channels that open within milliseconds upon agonist binding, $P2X_7$ receptors induce formation of a large pore, activation of the inflammasome, and numerous other downstream signaling events in response to prolonged stimulation (1, 19–22).

The functional expression level of $P2X_7$ receptor is crucial in its role in the disease pathogenesis. This has been highlighted by an increasing number of findings that aberrant or altered receptor expression and function have a causative role in chronic lymphocytic leukemia (8, 23, 24), reduced bacterial-killing ability of macrophages (26, 27), impaired release of cytokines (6, 28–30), inflammatory and neuropathic pain (11, 16), rheumatoid arthritis (7), neurodegenerative and neuroinflammatory disorders (13, 14, 31–36), mood-depressive disorders (37–40), and epithelial cancers (41–43). Studies of the mammalian $P2X_7$ receptors, and particularly the human (h) and rat (r) $P2X_7$ receptors, have revealed striking species differences in the receptor properties, including receptor-mediated functional responses and sensitivities to agonists, antagonists, and modulators (19–21, 44–52). However, the physiological implications and underlying mechanisms are still not well understood.

Our recent study characterizing the mutations resulting from non-synonymous SNPs in the human *P2RX7* gene has shown that H155Y and A348T mutations increase ATP-induced currents (53). These two gain-of-function mutations substitute the residues in the $hP2X_7$ receptor with the corre-

* This work was supported in part by the Biotechnology and Biological Science Research Council.

[S] The on-line version of this article (available at http://www.jbc.org) contains supplemental Figs. S1–S6.

[1] Recipient of a Biotechnology and Biological Science Research Council Ph.D. studentship.

[2] Both authors contributed equally to this work.

[3] To whom correspondence should be addressed. E-mail: l.h.jiang@leeds.ac.uk.

[4] The abbreviations used are: BzATP, benzoylbenzoyl-ATP; h, human; r, rat; ER, endoplasmic reticulum; pF, picofarads.

sponding ones in the rP2X$_7$ receptor. Here, we show evidence for a critical role of residues at positions 155 and 348 in determining the ATP-induced currents mediated by hP2X$_7$ and rP2X$_7$ receptors and the distinct mechanisms that underlie their contribution.

MATERIALS AND METHODS

Cell and Molecular Biology—Human embryonic kidney HEK293 cells were used to transiently express WT and mutant P2X$_7$ receptors. Cell preparation and transfection using Lipofectamine 2000 reagent (Invitrogen) were performed according to the manufacturer's instructions. In brief, for patch-clamp recordings, HEK293 cells in a 35-mm Petri dish were cotransfected with 1 μg of P2X$_7$ plasmid and 0.1 μg of enhanced GFP plasmid or otherwise as specifically indicated. Cells were dispersed on coverslips 12–24 h after transfection and used within 48 h. The transfection efficiency, estimated based on the GFP-positive cells, was >50%, and single cells with similar GFP expression levels were used. For biotin labeling and immunostaining, HEK293 cells were transfected in the same way except for omission of GFP plasmid for immunostaining experiments. The cDNAs encoding the rP2X$_7$ (Swiss-Prot accession number Q64663) and hP2X$_7$ (accession number Q99572) proteins with a C-terminal EYMPME (referred to as EE) epitope were inserted in the pcDNA3 or pcDNA3.1 vector (Invitrogen). Mutations were introduced by site-directed mutagenesis and confirmed by sequencing.

Patch-Clamp Recording—Whole-cell currents were recorded at room temperature as described previously (54) using an HEKA EPC 10 amplifier at a holding potential of −60 mV. Normal extracellular solution contained 147 mM NaCl, 2 mM KCl, 1 mM $MgCl_2$, 2 mM $CaCl_2$, 10 mM HEPES, and 13 mM glucose (pH 7.3). The maximal currents in cells expressing P2X$_7$ receptors were not readily observed in the normal solution by applying 5–10 mM ATP (53), and therefore, most experiments were carried out in low divalent cation extracellular solution containing no $MgCl_2$ and 0.3 mM $CaCl_2$. Intracellular solution contained 145 mM NaCl, 10 mM EGTA, and 10 mM HEPES (pH 7.3). The currents were compared upon full facilitation (51) by repeated applications of submaximal concentrations of agonist every 1 min. Bisperoxo(1,10-phenanthroline)oxovanadate (V) (100 μM) was used to mitigate current decline in some experiments (55). The concentration-current response curves shown in the figures were constructed using the recordings that showed <10% decline in the currents induced by the same concentration of agonists used for facilitation before and after measuring the concentration-current responses. To examine each subset of mutations, only the data for the WT receptor obtained in parallel experiments were used for comparison. To test the KN-62 antagonist, currents induced by 1 mM ATP, when reproducible, were exposed to each accumulative concentration for 4 min. The ATP concentration-current responses were also measured before and 4 min after exposure to 100 nM KN-62. Agonists and antagonists were delivered using a Bio-Logic RSC160 system.

Structural Modeling—The structural model of the hP2X$_7$ receptor was generated based on the crystal structure of the zebrafish P2X$_4$ receptor (Protein Data Bank code 3H9V) (56). As we have described recently (53), the modeling was carried out using Modeler Version 8.2 (57). The non-conserved loop region between the β2 and β3 strands was modeled *de novo* using the ModLoop server (58, 59). Images were generated using UCSF Chimera Version 1.4 (60).

Immunofluorescence Confocal Imaging—These experiments were carried out as detailed previously (61, 62). To examine the subcellular distribution of the WT and mutant P2X$_7$ receptor proteins, cells were stained with rabbit anti-EE primary antibody (1:500 or 1:000 dilution; Bethyl) for 2–3 h (or overnight at 4 °C) and Alexa Fluor 488-conjugated anti-rabbit IgG secondary antibody (1:4000 or 1:500; Molecular Probes) for 1–2 h. To examine the co-localization of hP2X$_7$ proteins and calreticulin, an endoplasmic reticulum (ER) protein marker, cells transfected with hP2X$_7$ plasmid were first stained with mouse anti-calreticulin primary antibody (1:250; Stressgen) overnight at 4 °C and FITC-conjugated goat anti-mouse IgG secondary antibody (1:500; Sigma) for 2 h. Cells were then stained with rabbit anti-EE primary antibody (1:500) for 3 h and Alexa Fluor 546-conjugated goat anti-rabbit IgG secondary antibody (1:500; Molecular Probes) for 2 h. To examine the co-localization of hP2X$_7$ proteins and LAMP1 (lysosome-associated membrane protein 1) in the late endocytic organelles (late endosomes and lysosomes), cells were cotransfected with 1 μg of hP2X$_7$ plasmid and 0.5 μg of plasmid encoding LAMP1 fused at its C terminus to GFP (GFP-LAMP1) and stained with rabbit anti-EE primary antibody (1:1000 or 1:2000) for 3 h and Cy3-conjugated goat anti-rabbit IgG secondary antibody (1:2000; Molecular Probes) for 2 h. To examine the co-localization of hP2X$_7$ proteins and TGN46, a *trans*-Golgi network protein, cells transfected with hP2X$_7$ plasmid were stained with sheep anti-TGN46 primary antibody (1:100) overnight at 4 °C and FITC-conjugated donkey anti-sheep IgG secondary antibody (1:100; Jackson ImmunoResearch Laboratories) for 2 h. Cells were then stained with rabbit anti-EE primary antibody (1:1000 or 1:2000) for 3 h and Cy3-conjugated goat anti-rabbit IgG secondary antibody (1:2000) for 2 h. The images were captured using a Zeiss Axiovert 200M confocal microscope and LSM 150 META software or a Nikon Eclipse TE2000-E confocal microscope and NIS-Elements AR software.

Biotin Labeling and Western Blotting—Biotin labeling was performed by modifying the protocols described previously (62, 63). In brief, cells transfected with P2X$_7$ plasmid (or an empty vector) and GFP plasmid were labeled with sulfo-NHS-LC-biotin (Pierce) for 30 min at 4 °C. Total protein concentrations of the cell lysates were determined using the BCA assay (Thermo Scientific). The biotinylated proteins were purified from a total of 300 μg of lysates using EZview red streptavidin affinity beads (Sigma) overnight at 4 °C and eluted in 50 μl of electrophoresis sample buffer (6% SDS, 10% glycerol, 50 mM Tris-HCl (pH 6.8), 2 mM EDTA, 0.05% bromphenol blue, and 10% β-mercaptoethanol). Whole-cell lysate (5 or 10 μg) or biotin-labeled samples (20 μl) were separated on 12% SDS-polyacrylamide gels. Proteins were detected using rabbit anti-EE primary antibody (1:5000) or mouse anti-GFP antibody (1:2000; Santa Cruz Biotechnology) and horseradish peroxidase-conjugated anti-rabbit secondary antibody (1:5000; Santa Cruz Biotechnology) or anti-mouse IgG antibody (1:2000; Santa Cruz Biotechnology)

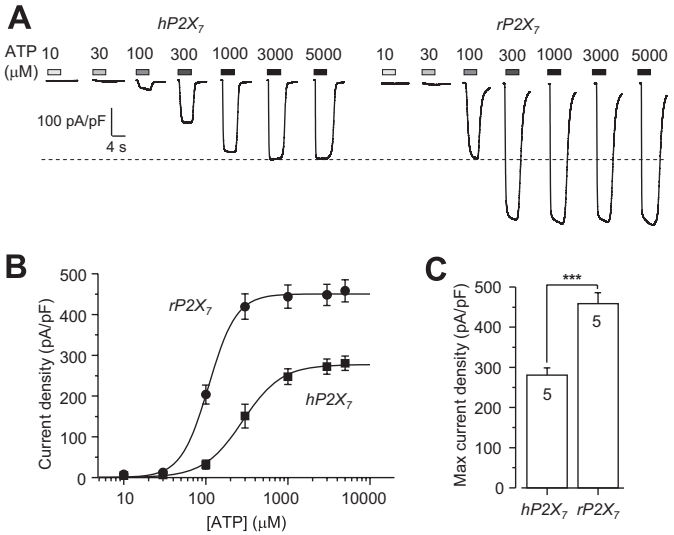

FIGURE 1. **ATP-induced current responses mediated by the hP2X$_7$ and rP2X$_7$ receptors.** *A*, representative ATP-induced inward current densities in cells expressing the hP2X$_7$ (*left*) or rP2X$_7$ (*right*) receptor. The *dashed line* denotes the maximal current for the hP2X$_7$ receptor. *B*, ATP concentration-current density curves from recordings shown in *A*. *Lines* represent the best fits to the Hill equation. *C*, mean maximal current density in parallel experiments. The cell number in each case for *B* and *C* is indicated in *C*. ***, $p < 0.001$ compared between the hP2X$_7$ and rP2X$_7$ receptors (*t* test).

and visualized using SuperSignal West Femto maximal sensitivity substrate (Thermo Scientific).

Data Analysis—All results, where appropriate, are presented as means ± S.E. All currents are presented as current density, *i.e.* the currents divided by the cell capacitance, to minimize the effects of the variation in cell size. Agonist EC_{50} values were determined by least-squares fitting of the data from individual cells to the Hill equation: $I = I_{max}/(1 + (EC_{50}/[A])^n)$, where I is the peak current density evoked by given agonist concentrations ([A]), I_{max} is the maximal current density, and n is the Hill coefficient. Figures show the curves fitted to the mean of all experiments. Antagonist IC_{50} values were derived by fitting the data from individual cells to the Hill equation: $I = 100/(1 + ([B]/IC_{50})^n)$, where I is the ATP-induced currents after exposure to given concentrations of antagonist ([B]) expressed as a percentage of the control currents before antagonist application, and n is the Hill coefficient. Curve fits were performed using Origin software. Statistical analysis was carried out using Student's *t* test for two groups and one-way analysis of variance test for more than two groups, and the difference was considered to be significant at $p < 0.05$.

RESULTS

Initial Comparison of hP2X$_7$ and rP2X$_7$ Receptor-mediated ATP-induced Currents—ATP is the physiological agonist for all P2X receptors, including the P2X$_7$ receptor. Fig. 1*A* shows representative currents responses of cells expressing WT hP2X$_7$ and rP2X$_7$ receptors to the indicated concentrations of ATP recorded in low divalent cation extracellular solution (see "Materials and Methods"). Two differences are discernible. First, the hP2X$_7$ receptor was less sensitive to ATP than the rP2X$_7$ receptor, with EC_{50} values of 304 ± 49 μM ($n = 5$) and 110 ± 6 μM ($n = 5$; $p < 0.01$) for the human and rat receptors, respectively (Fig. 1*B*). Second, the amplitude of currents mediated by the hP2X$_7$ receptor was lower than that mediated by the rP2X$_7$ receptor. The average current density evoked by the maximal concentration of ATP (I_{max}) was 281 ± 18 pA/picofarads (pF; $n = 5$) for the hP2X$_7$ receptor, corresponding to ~60% of the value of 458 ± 27 pA/pF ($n = 5$; $p < 0.001$) obtained for the rP2X$_7$ receptor (Fig. 1*C*). These results provide an initial indication of significant functional differences between these two receptors.

Reciprocal Substitution of Residues at Positions 155 and 348 in the hP2X$_7$ and rP2X$_7$ Receptors—To test whether residues at positions 155 and 348 are involved in determining the P2X$_7$ receptor function, and particularly the difference between human and rat receptors, we compared the ATP-induced currents mediated by hP2X$_7$ and rP2X$_7$ receptors bearing reciprocal mutations in low divalent cation extracellular solution. Fig. 2*A* shows representative ATP-induced currents in cells expressing the WT or mutant hP2X$_7$ receptors. The A348T and H155Y mutations caused little or no change in the ATP sensitivity of the receptor (Fig. 2*B*). However, the ATP-induced I_{max} increased from 268 ± 12 pA/pF ($n = 29$) for the WT receptor to 391 ± 19 pA/pF ($n = 10$; $p < 0.001$) for the H155Y mutant and 324 ± 17 pA/pF ($n = 12$; $p < 0.05$) for the A348T mutant (Fig. 2*C*). These results confirmed our recent report that both the H155Y and A348T mutations increase hP2X$_7$-mediated ATP-induced responses (53). The ATP-induced I_{max} was further increased by the double mutation H155Y/A348T (473 ± 31 pA/pF ($n = 7$); $p < 0.001$); the increase was significantly greater than that produced by the single mutations (Fig. 2*C*).

Fig. 3*A* shows representative ATP-induced currents under the same experimental conditions, resulting from expression of the WT rP2X$_7$ receptor or the Y155H, T348A, or Y155H/T348A mutants. The T348A mutation did not alter the ATP sensitivity, whereas the Y155H and Y155H/T348A mutations caused small reductions (~3- and 5-fold increases in the EC_{50} value, respectively) (Fig. 3*B*). The most prominent mutational effect was that the ATP-induced I_{max} was strongly attenuated from 444 ± 24 pA/pF ($n = 10$) for the WT receptor to 211 ± 25 pA/pF ($n = 7$; $p < 0.001$) for the Y155H mutant and 326 ± 23 pA/pF ($n = 7$; $p < 0.01$) for the T348A mutant (Fig. 3*C*). The ATP-induced I_{max} was further reduced by the double mutation Y155H/T348A (114 ± 18 pA/pF ($n = 3$); $p < 0.001$); the reduction was significantly greater than that yielded by the single mutations (Fig. 3*C*). We also examined ATP-induced currents mediated by the WT rP2X$_7$ receptor and the Y155H and T348A mutants in a solution with normal extracellular divalent cation concentrations (see "Materials and Methods"). The reduction in the ATP-induced I_{max} caused by the Y155H and T348A mutations was also clear under these conditions (supplemental Fig. S1), in striking contrast with the increase in the ATP-induced I_{max} resulting from the H155Y and A348T mutations in the hP2X$_7$ receptor under the same conditions, as reported in our recent study (53). These contrasting effects were also apparent in terms of BzATP-induced currents. The H155Y and A348T mutations in the hP2X$_7$ receptor increased and the reciprocal Y155H and T348A mutations in the rP2X$_7$ receptor reduced the BzATP-induced I_{max} (supplemental Fig. S2).

All these results consistently indicated that reciprocal mutations of residues at positions 155 and 348 essentially switched

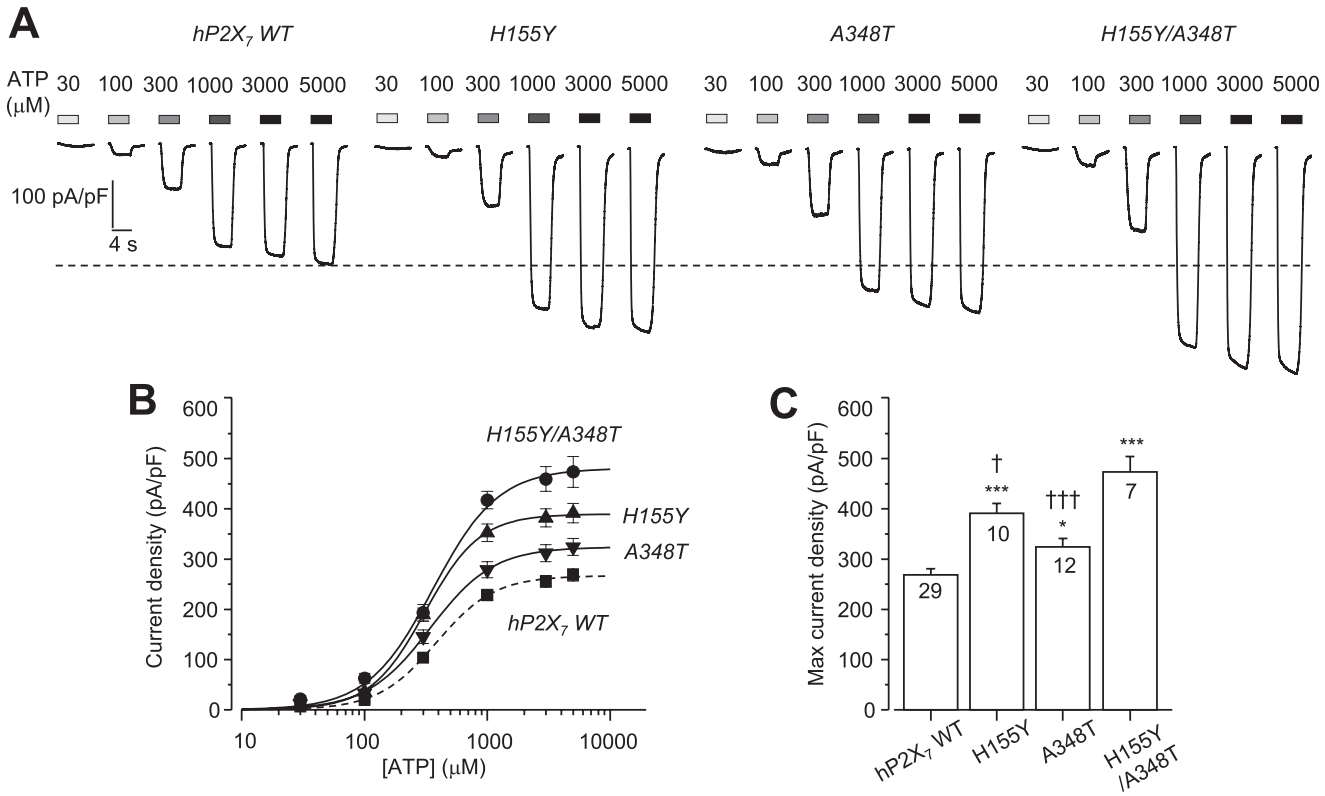

FIGURE 2. **Effects of H155Y and A348T mutations on ATP-induced currents mediated by the hP2X$_7$ receptor.** *A*, representative ATP-induced current densities in cells expressing the WT hP2X$_7$ receptor or the H155Y, A348T, or H155Y/A348T mutant. The *dashed line* denotes the maximal current for the WT hP2X$_7$ receptor. *B*, ATP concentration-current density curves from recordings shown in *A*. The *lines* represent the best fits to the Hill equation. The *dashed line* denotes the WT hP2X$_7$ receptor. *C*, mean maximal current density in parallel experiments. The cell number in each case for *B* and *C* is indicated in *C*. ***, $p <$ 0.001, and *, $p < 0.05$ compared with the WT receptor; †††, $p < 0.001$, and †, $p < 0.05$ compared with the H155Y/A348T double mutant receptor (*t* test).

the agonist-induced current responses mediated by the hP2X$_7$ and rP2X$_7$ receptors. Such findings strongly suggest a critical role for these two residues in determining the P2X$_7$ receptor function and, in particular, the difference in the current responses between human and rat receptors.

Further Substitution of His-155 and Ala-348 in the hP2X$_7$ Receptor—To gain more insight into the role of residues at positions 155 and 348 and to test the importance of the side chain, we mutated His-155 and Ala-348 in the hP2X$_7$ receptor to residues with side chains that have diverse properties (small, lengthy, bulky, neutral, or negatively or positively charged). Fig. 4 shows representative ATP-induced currents and the concentration-response curves in cells expressing the hP2X$_7$ receptors carrying mutations of His-155 (Fig. 4, *A* and *B*) and Ala-348 (Fig. 4, *C* and *D*), respectively. Overall, there was no or a small change in the ATP sensitivity for all mutants (Fig. 4, *B* and *D*). The ATP-induced I_{max} was reduced by the H155L and H155D mutations but was not changed by the H155A, H155N, H155R, and H155F mutations (Fig. 4*E*). In contrast, the ATP-induced I_{max} was significantly altered by each residue substituted for Ala-348 (Fig. 4*F*). Although the effects of mutations showed no clear relationship to the size of the residues introduced into His-155 (Fig. 4*E*), there was an apparent correlation between the effects of mutations and the volume of the residues used to replace Ala-348 (Fig. 4*F*): the one with the smallest side chain (A348G) conferred the greatest increase in the ATP-induced I_{max}, and the ones with the larger side chains (A348M and A348F) caused the greatest decrease. These results show a strong dependence of the effects of mutations on the side chains, suggesting that the side chain properties of residues at positions 155 and 348 are critical in determining the P2X$_7$ receptor function.

Substitutions of Residues Surrounding His-155 and Ala-348 in the hP2X$_7$ Receptor—Several residues surrounding positions 155 and 348 are different between the hP2X$_7$ and rP2X$_7$ receptors (Fig. 5*A*). To investigate whether any of these residues have a similar role, we individually replaced the residues in the hP2X$_7$ receptor with the corresponding ones in the rP2X$_7$ receptor and examined the effects on the ATP-induced currents. Swapping residues in the region surrounding His-155 resulted in six mutants: V153I, V154P, E156D, G157Q, N158K, and Q159R. Fig. 6*A* shows their ATP concentration-response curves (see representative currents in supplemental Fig. S3*A*). The G157Q and Q159R mutations reduced the ATP-induced I_{max}, whereas the other mutations had no effect. We also introduced tyrosine into positions 154 and 156, flanking His-155. Fig. 6*B* shows the results (see representative currents in supplemental Fig. S3*B*). Unlike H155Y, the V154Y mutation had no effect on the ATP-induced I_{max}, whereas the E156Y mutation strongly decreased it (Fig. 6*D*). These results indicate that none of these mutations mimics H155Y or that none of these residues has a role similar to that of His-155. Fig. 6*C* summarizes the results from swapping the four residues in the region surrounding Ala-348 (see representative currents in supplemental Fig. S3*C*). The F350C and L354I mutations were without effect. However, the D356N mutation reduced and the F353L muta-

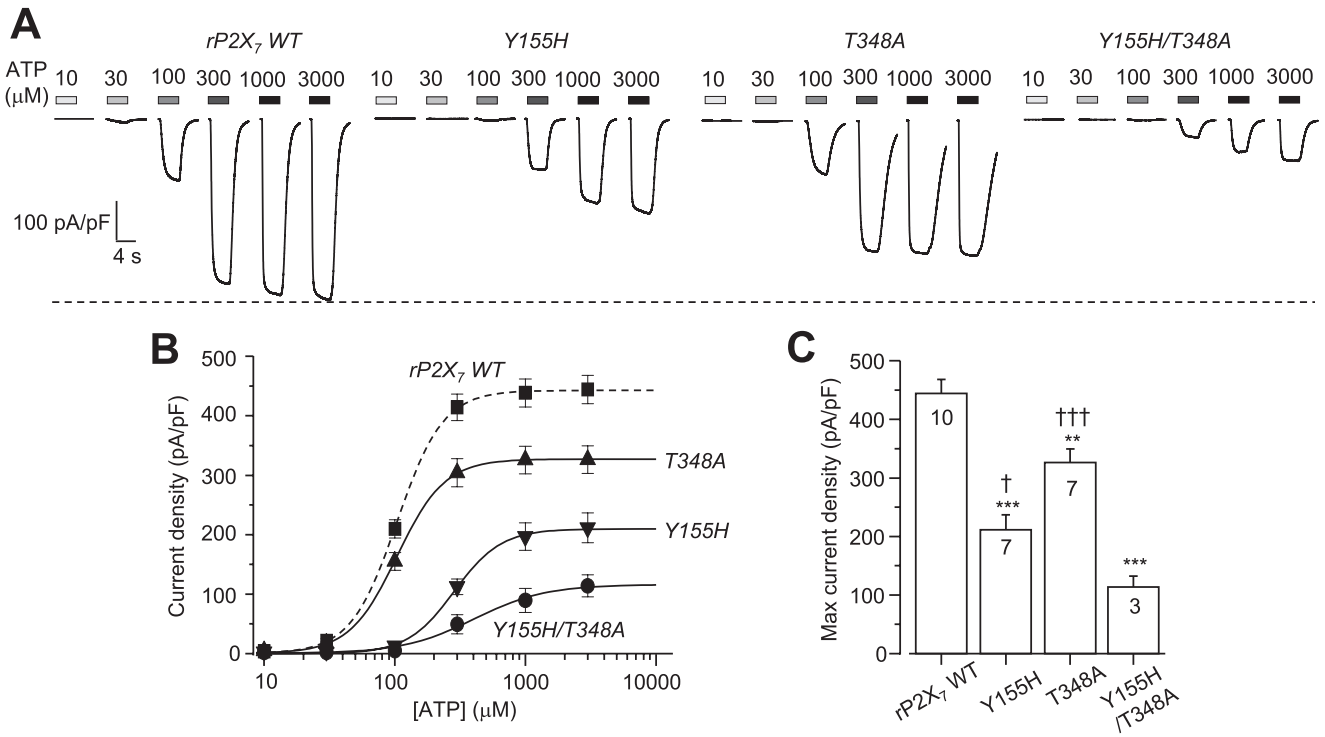

FIGURE 3. **Effects of Y155H and T348A mutations on ATP-induced currents mediated by the rP2X$_7$ receptor.** *A*, representative ATP-induced current densities in cells expressing the WT rP2X$_7$ receptor or the Y155H, T348A, or Y155H/T348A mutant. The *dashed line* denotes the maximal current for the WT rP2X$_7$ receptor. *B*, ATP concentration-current density curves from recordings shown in *A*. The *lines* represent the best fits to the Hill equation. The *dashed line* denotes the WT rP2X$_7$ receptor. *C*, mean maximal current density in parallel experiments. The cell number in each case for *B* and *C* is indicated in *C*. ***, $p < 0.001$, and **, $p < 0.01$ compared with the WT receptor; †††, $p < 0.001$, and †, $p < 0.05$ compared with the Y155H/T348A double mutant receptor (*t* test).

tion increased the ATP-induced I_{max} (Fig. 6*D*). However, introduction of the reciprocal L353F mutation into the rP2X$_7$ receptor had no significant effect (data not shown). Taken together, the results from these experiments suggest that His-155 and Ala-348 and also some surrounding residues, including Glu-156, Gly-157, Gln-159, Phe-353, and Asp-356, are involved in determining the hP2X$_7$-mediated ATP-induced current responses. However, only residues at positions 155 and 348 are critical for the difference between hP2X$_7$ and rP2X$_7$ receptors.

Effects of Mutating Residues at Positions 155 and 348 on Cell-surface Expression of the P2X$_7$ Receptors—Whole-cell ionic currents are governed by two distinctive factors: the number of functional channels at the cell surface (surface expression) and the single-channel function (conductance and opening probability) (65). We therefore investigated whether residues at positions 155 and 348 are important in determining the surface expression of the hP2X$_7$ and rP2X$_7$ receptors. Using immunofluorescence confocal imaging, we compared the subcellular distribution of the WT and mutant human and rat receptors containing reciprocal mutations of residues at these two positions. Fig. 7*A* shows representative results. The immunoreactivity for the WT hP2X$_7$ proteins was highly diffused. This diffuse distribution was largely retained for the A348T mutant. In contrast, the immunoreactivity for the H155Y mutant was highly enriched on or near the cell surface (Fig. 7*A*, *left panels*). On the other hand, the immunoreactivity for the WT rP2X$_7$ proteins was located principally within or in close vicinity of the plasma membrane, as we reported previously (54, 66). Such membrane-restricted immunostaining was strongly disrupted by the Y155H mutation and only slightly reduced by the T348A mutation (Fig. 7*A*, *right panels*).

To further examine the effects of mutations on cell-surface expression, we used biotin labeling and Western blotting to analyze surface and total protein expression of the WT and mutant hP2X$_7$ and rP2X$_7$ receptors. Fig. 7*B* shows representative results. The H155Y mutation increased the surface protein expression (*upper panel*) and also increased the total protein expression (*lower panel*) of the hP2X$_7$ receptor. However, there was no change in the control GFP protein expression (*lower panel*). We also examined the H155N mutation, which did not change the ATP-induced I_{max} (Fig. 4*E*), and found that unlike the H155Y mutation, the H155N mutation had no effect on the surface and total protein expression (supplemental Fig. S4). In contrast with the H155Y mutation in the hP2X$_7$ receptor, the reciprocal Y155H mutation strongly reduced the surface protein expression and, to a lesser degree, the total protein expression of the rP2X$_7$ receptor (Fig. 7*B*). However, such contrasting changes in the surface and total protein expression were not observed for the A348T mutation in the hP2X$_7$ receptor and the T348A mutation in the rP2X$_7$ receptor (Fig. 7*B*), consistent with the immunostaining results (Fig. 7*A*).

Therefore, our results show that the H155Y mutation in the hP2X$_7$ receptor enhanced the surface expression of the protein and conferred a subcellular distribution close to that of the WT rP2X$_7$ receptor. Conversely, the reciprocal mutation Y155H in the rP2X$_7$ receptor decreased the surface expression and resulted in a subcellular distribution that was similar to that of the WT hP2X$_7$ receptor. There was no such effect on both

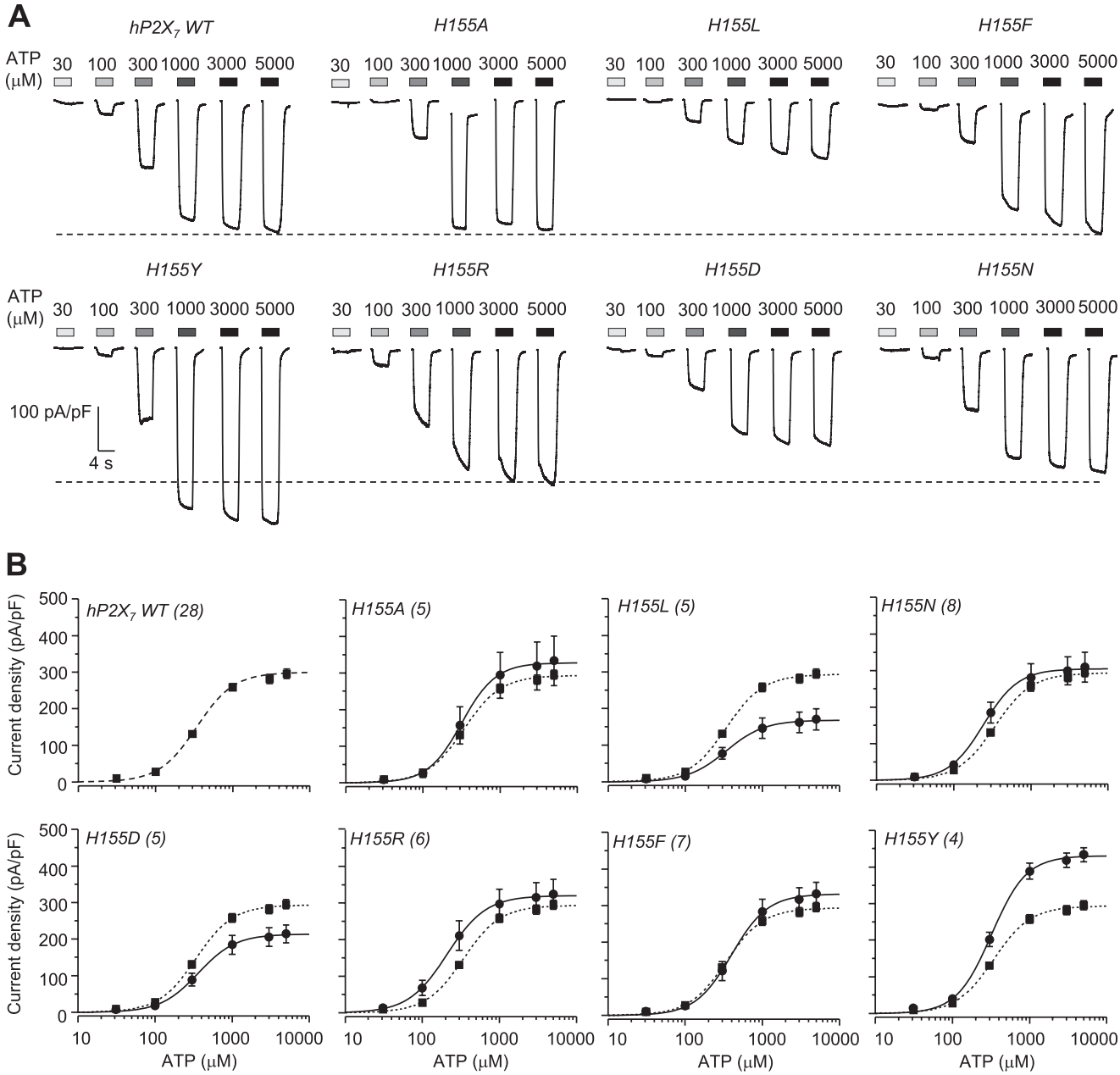

FIGURE 4. **Mutational analysis of the roles of residues at positions 155 and 348 in the hP2X$_7$ receptor.** *A*, representative ATP-induced current densities in cells expressing the WT hP2X$_7$ receptor and mutant receptors carrying mutations of His-155. *B*, ATP concentration-current density curves from recordings shown in *A*. *C*, representative ATP-induced current densities in cells expressing the WT hP2X$_7$ receptor and mutant receptors carrying mutations of Ala-348. *D*, ATP concentration-current density curves from recordings shown in *C*. In *A* and *C*, the *dashed lines* denote the maximal currents for the WT hP2X$_7$ receptor. In *B* and *D*, the *lines* represent the best fits to the Hill equation, and the *dashed lines* denote the WT hP2X$_7$ receptor. The number of cells examined in each case is indicated in *parentheses*. *E* and *F*, the mean maximal current density from *A–D* is plotted against the volume of the amino acid residues (from Ref. 25) introduced into positions 155 (*E*) and 348 (*F*). The *dashed lines* denote the mean maximal currents for the WT hP2X$_7$ receptor in parallel experiments. ***, $p < 0.001$, **, $p < 0.01$, and *, $p < 0.05$ compared with the WT hP2X$_7$ receptor (*t* test). In F, # indicates that A348G differs from the WT receptor, A348M, and A348F; A348T differs from A348M and A348F; A348M differs from A348G and A348T; and A348F differs from A348G and A348T (one-way analysis of variance test, $p < 0.05$). The *solid line* shows a linear fit, and the *R* value is 0.7.

subcellular distribution and surface expression by the reciprocal mutations of residue 348. These results, together with the effects of mutations on the ATP-induced I_{max}, imply an important role for residue 348 in determining the single-channel function and provide direct evidence to support a critical role for residue 155 in surface expression. As discussed below, such interpretations are consistent with the structural model of the hP2X$_7$ receptor based on the recently published crystal structure of the zebrafish P2X$_4$ receptor (55).

Subcellular Localization of Intracellular hP2X$_7$ Receptor Proteins—Immunofluorescence confocal imaging showed extensive intracellular location of the hP2X$_7$ receptor proteins (Fig. 7*A*). To investigate in which subcellular compartments they might be located, we performed double immunostaining of hP2X$_7$ proteins and intracellular organelle marker proteins. Fig. 8 shows representative confocal images. There was strong co-localization of the hP2X$_7$ proteins with calreticulin, an ER protein marker (Fig. 8*A*), but not with TGN46, a *trans*-Golgi

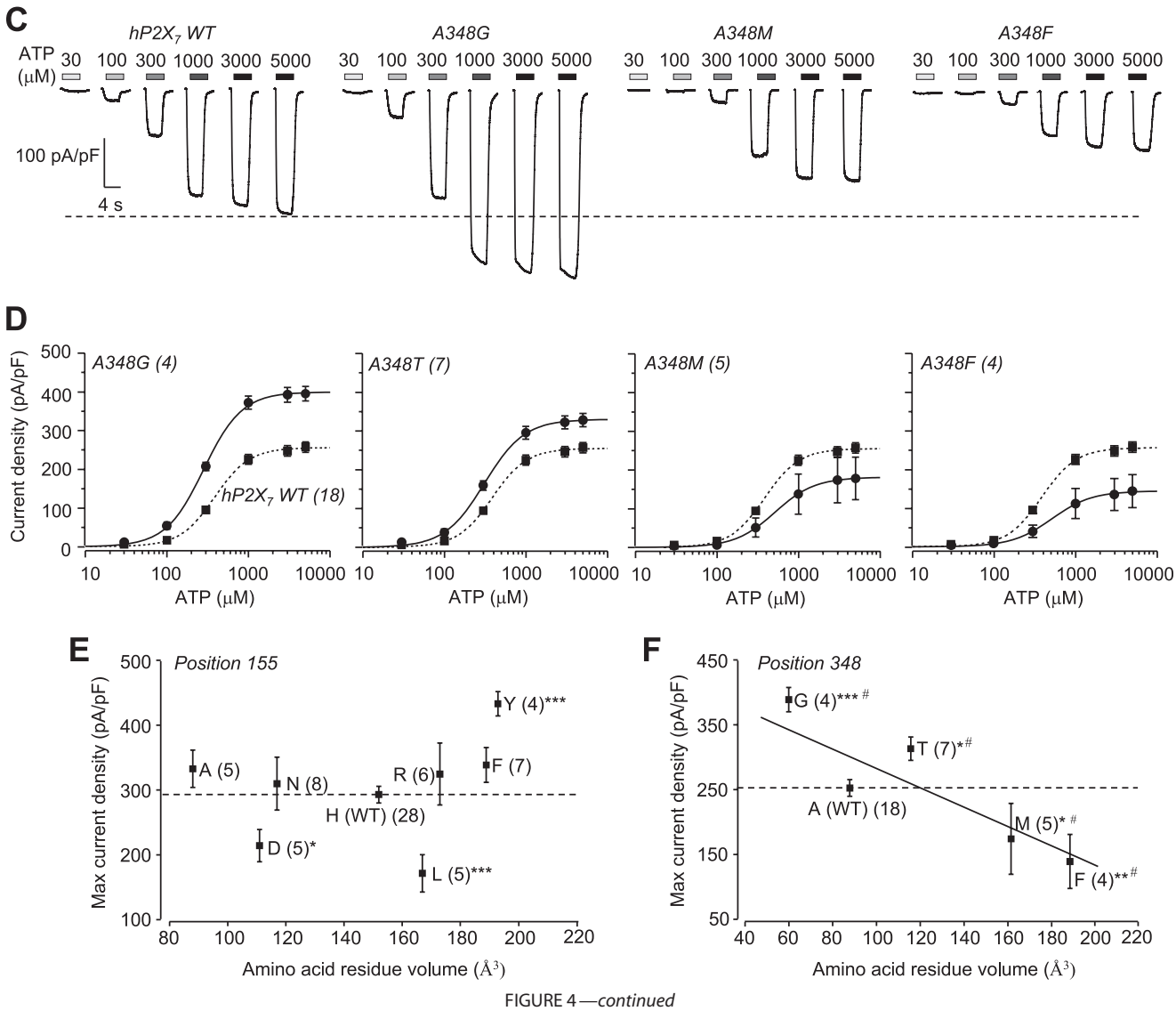

FIGURE 4—*continued*

network protein marker (Fig. 8*B*). In addition, the immunoreactivity for the hP2X$_7$ proteins exhibited no apparent co-localization with the coexpressed GFP-LAMP1, a protein localized to the late endocytic compartments and lysosomes (supplemental Fig. S6). These results indicate that the intracellular hP2X$_7$ proteins reside mainly within the ER.

DISCUSSION

By combining site-directed mutagenesis with whole-cell current patch-clamp recording and protein expression assays, we have shown that the residues at positions 155 and 348 are critical in determining ATP-induced currents mediated by P2X$_7$ receptors, as well as the difference between the human and rat receptors. We have provided further evidence to suggest that distinct molecular mechanisms underlie their contribution.

Importance of Residues at Positions 155 and 348 in Determining the P2X$_7$ Receptor Function—The gene encoding the hP2X$_7$ receptor has extensive SNPs (650 in total as of today), including many non-synonymous ones, several of which have been shown to alter the receptor functions (23, 24, 26–29, 53–55, 61, 64, 67–78). H155Y and A348T are unique in that both mutations change residues in the hP2X$_7$ receptor to the corresponding ones in the rP2X$_7$ receptor (Fig. 5*A*). Interestingly, these two mutations confer gain of function (Fig. 2) (53, 67), hinting that Tyr-155 and Thr-348 may contribute to the greater currents mediated by the rP2X$_7$ receptor than those by the hP2X$_7$ receptor (Fig. 1). The results from studying the hP2X$_7$ and rP2X$_7$ receptors bearing the reciprocal mutations show that such swapping of residues at positions 155 and 348 results in opposite effects on the ATP-induced I_{max} (Figs. 2 and 3), providing compelling evidence to indicate that the residues at positions 155 and 348 are important in determining the hP2X$_7$ and rP2X$_7$ receptor functions.

The effects of mutating His-155 on the ATP-induced I_{max} clearly depend on the introduced residues, but there was no clear correlation between the side chain properties of the residues and the functional phenotypes (Fig. 4*E*). For example, phenylalanine also contains a bulky side chain but failed to mimic tyrosine (Fig. 4*E*). In contrast, the effects of mutating Ala-348 on the ATP-induced I_{max} showed a clear correlation with the

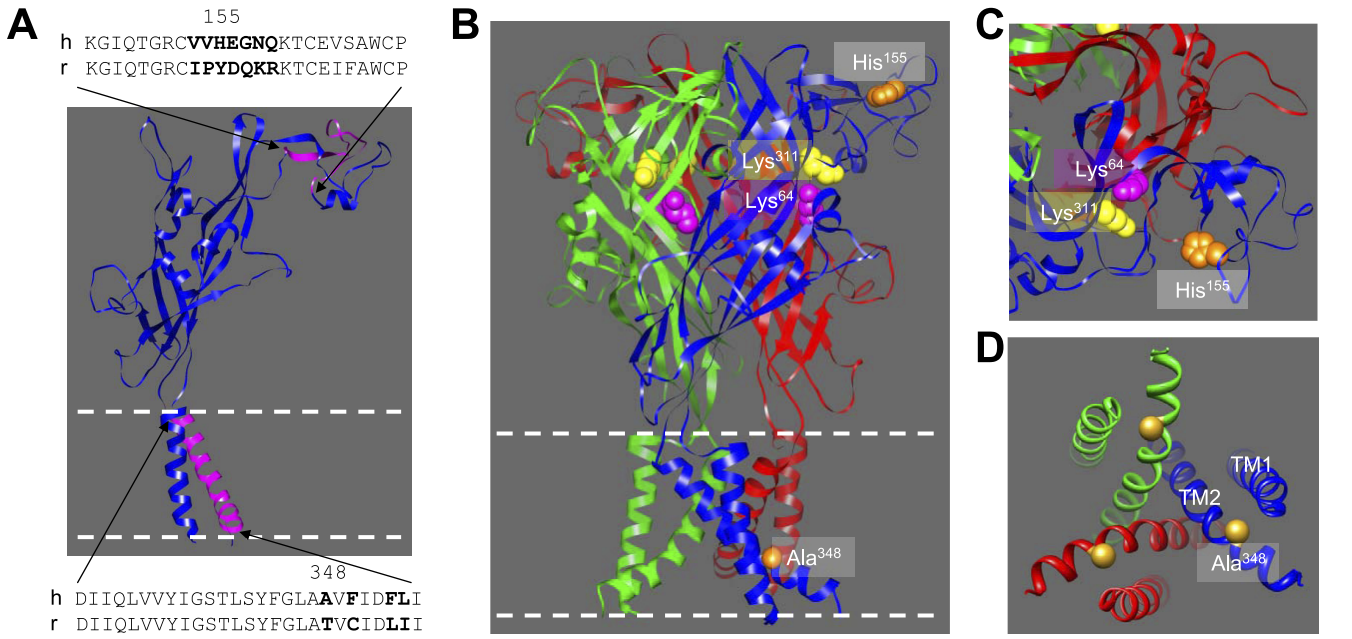

FIGURE 5. **Structural model of hP2X$_7$ receptors and locations of His-155 and Ala-348.** *A*, the dolphin-shaped structural model of a single hP2X$_7$ subunit, with the residues surrounding positions 155 and 348 highlighted in *purple* and those under investigation denoted in *boldface* in the sequences. *B*, the trimeric complex of the hP2X$_7$ receptor, with three different subunits in *blue*, *green*, and *red*, respectively. His-155 and Ala-348 are shown in *orange*. Lys-64 (in *purple*) and Lys-311 (in *yellow*) represent the key residues in the intersubunit ATP-binding site. The structures in *A* and *B* are viewed parallel to the membrane plane. *C*, a snapshot of the structure surrounding His-155, viewed from along the axis of 3-fold symmetry from the extracellular side. His-155 is distant from the ATP-binding site. *D*, a snapshot of the structure surrounding Ala-348, viewed from along the axis of 3-fold symmetry from the intracellular side. TM2 contributes the ion-conducting pathway, and TM1 is largely peripheral. Ala-348 is positioned immediately intracellularly to the narrowest part (the gate) of the ion-conducting pathway.

side chain size of the introduced residues (Fig. 4*F*). Swapping residues surrounding His-155 and Ala-348 identified several other residues, including Glu-156, Gly-157, Gln-159, Phe-353, and Asp-356, that influence the hP2X$_7$-mediated ATP-induced currents, but none of these mutations were fully reminiscent of H155Y and A348T (Fig. 6*D*). These results show that the unique location and properties of the residues at positions 155 and 348 are critical in determining the P2X$_7$ receptor function.

Distinct Mechanisms Underlying the Contribution of Residues at Positions 155 and 348—The identification of residues 155 and 348 adds to the growing list of residues that contribute to determination of the P2X$_7$ receptor functional properties, but only in a few cases is the underlying mechanism clearly understood (23, 26–29, 53–55, 61, 64, 67–78). As mentioned above, the maximal agonist-induced whole-cell currents, which are widely used to indicate the functional expression of an ion channel, are determined by both the surface expression (channel number) and the single-channel function (conductance and opening probability) (64). Structural information proves powerful in helping to infer a mechanistic understanding of the P2X receptor functions from determined mutational effects, as we have reviewed recently (5). According to the structural model of the hP2X$_7$ receptor based on the crystal structure of the zebrafish P2X$_4$ receptor (Fig. 5) (56), His-155 is in the extracellular domain and is positioned at the periphery of the receptor complex and well away from the intersubunit ATP-binding site that contains the key residues Lys-64 and Lys-311 (Fig. 5, *B* and *C*) (5, 68). Consistent with this, mutating His-155 to residues with diverse side chain properties, despite significant alterations in the ATP-induced I_{max}, had no or a small effect on the ATP sensitivity (Fig. 4*B*). In addition, the H155Y mutant receptor exhibited virtually the same sensitivity to the hP2X$_7$-specific antagonist KN-62 (44) as the WT receptor (IC_{50} = 127 ± 38 nM (n = 3) for the WT receptor and 129 ± 20 nM (n = 3) for the H155Y mutant; $p > 0.1$). Furthermore, KN-62 at 100 nM resulted in almost identical inhibition of the ATP-induced currents mediated by the WT and H155Y mutant receptors (supplemental Fig. S5). These results strongly support the conclusion that the H155Y mutation causes no major changes in the global conformation (and particularly, the ligand-binding sites) of the receptor. Moreover, the location of His-155 is distant from the ion- permeating pathway (Fig. 5*B*). Thus, the functional results and structural considerations consistently disfavor significant involvement of residue 155 in determining the single-channel function and instead point to a role in the cell-surface expression of the receptor. Indeed, despite no indication of a change in the surface expression in a previous study using immunofluorescence flow cytometry (67), our immunofluorescence confocal imaging and biotin labeling studies clearly show that the H155Y mutation increases the surface expression of the hP2X$_7$ receptor, whereas the reciprocal mutation, Y155H, reduces the surface expression of the rP2X$_7$ receptor (Fig. 7). These results provide compelling evidence to support a role for residue 155 in determining the surface expression of the P2X$_7$ receptors. Residue 155 is expected to be located in the lumen of the ER and the *trans*-Golgi network before the receptor is inserted into the plasma membrane or inside the endosomes and lysosomes after retrieval from the cell surface. Our immunostaining results indicate that the intracellular hP2X$_7$ proteins reside mainly in the ER (Fig. 8). Thus, one

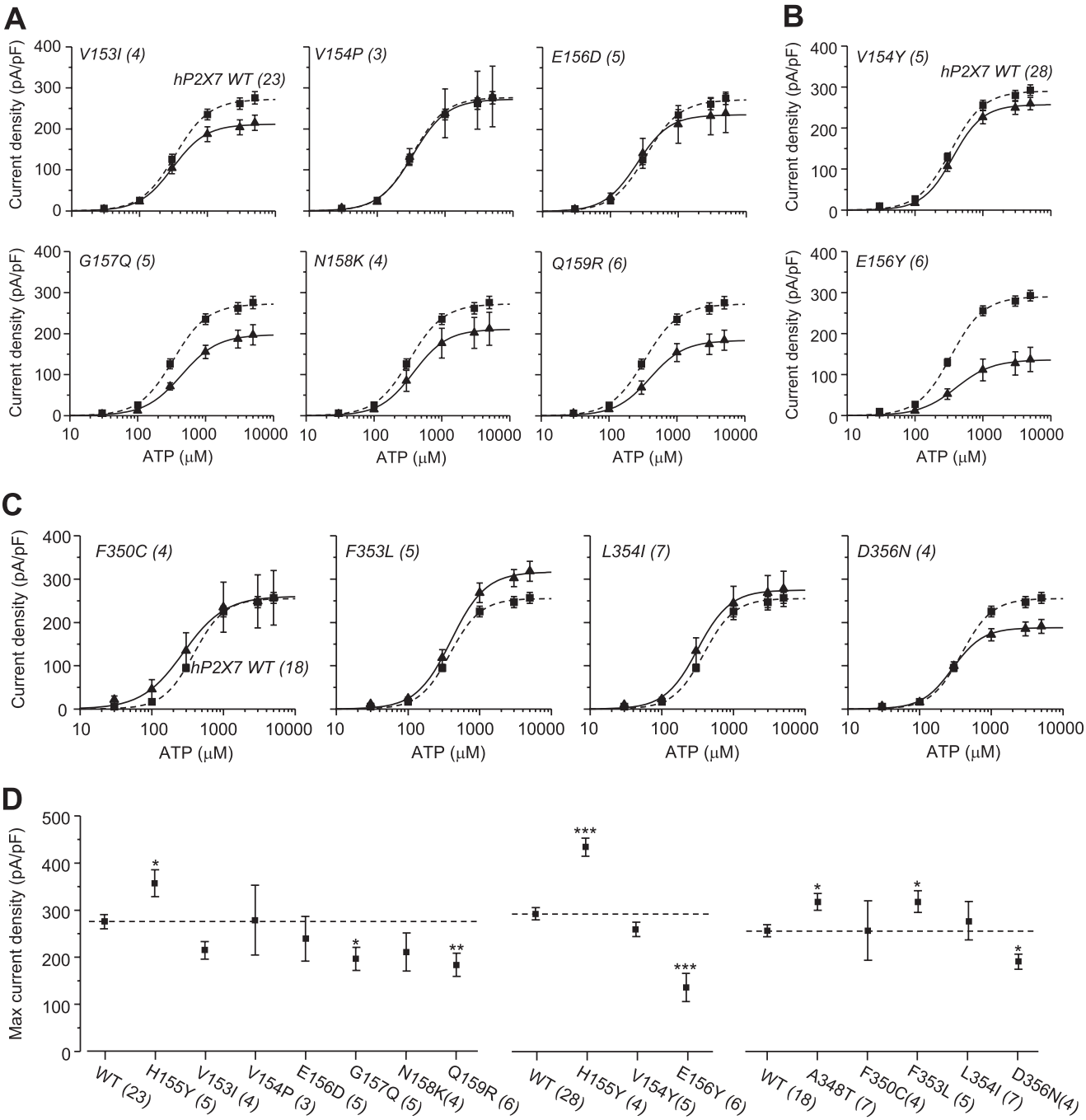

FIGURE 6. **Mutational analysis of residues surrounding His-155 and Ala-348 in the hP2X$_7$ receptor.** *A* and *B*, ATP concentration-current density curves for the hP2X$_7$ receptors carrying residue substitutions surrounding His-155. *C*, ATP concentration-current density curves for the hP2X$_7$ receptors carrying residue substitutions surrounding Ala-348. The lines represent the best fits to the Hill equation. The *dashed lines* denote the WT hP2X$_7$ receptor. The cell number in each case for *A–C* is indicated in *parentheses*. *D*, the mean maximal current density from *A–C*. The *dashed lines* denote the mean maximal currents for the WT hP2X$_7$ receptor in parallel experiments. ***, $p < 0.001$, **, $p < 0.01$, and *, $p < 0.05$ compared with the WT receptor (*t* test).

simple and consistent interpretation is that residue 155 is critical in the P2X$_7$ protein folding in the ER, resulting in P2X$_7$ receptors that are either transported from the ER to the plasma membrane or retained in the ER and degraded. This can also explain that mutation of residue 155 altered the total protein expression level (Fig. 7). However, we cannot exclude other possibilities such as altered protein synthesis or mRNA stability.

On the other hand, the model predicts Ala-348 to be part of the intracellular pore and close to the physical gate that occludes the ion-permeating pathway in the closed state (Fig. 5*D*) (5, 56), a position well purported for Ala-348 to have a role in channel gating and conductance. A recent study has proposed that a significant narrowing of the intracellular pore occurs during the P2X receptor channel opening (79). This notion is concordant with the strong correlation of the effects of mutating Ala-348 on the ATP-induced I_{max} with the side chain volume or size of the introduced residues (Fig. 4*F*). The immunofluorescence confocal imaging and biotin labeling results (Fig. 7)

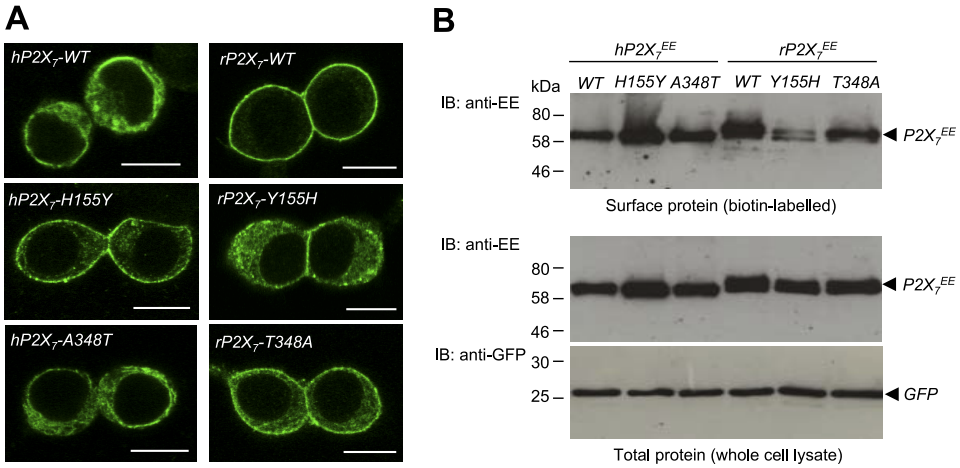

FIGURE 7. **Effect of reciprocal mutations of residues at positions 155 and 348 on subcellular distribution and the cell-surface and total expression of human and rat P2X$_7$ receptor proteins.** *A*, representative immunofluorescence confocal images of cells expressing the WT hP2X$_7$ receptor or the H155Y or A348T mutant (*left panels*) and the WT rP2X$_7$ receptor or the Y155H or T348A mutant (*right panels*). *Scale bars* = 10 μm. Similar results were observed in three independent experiments. *B*, representative Western blots showing cell-surface expression of the indicated P2X$_7$ proteins (biotin-labeled; *upper panel*) and total expression of the indicated P2X$_7$ and GFP proteins (whole-cell lysate; *lower panel*). Similar results were observed in two to five independent experiments. *IB*, immunoblot.

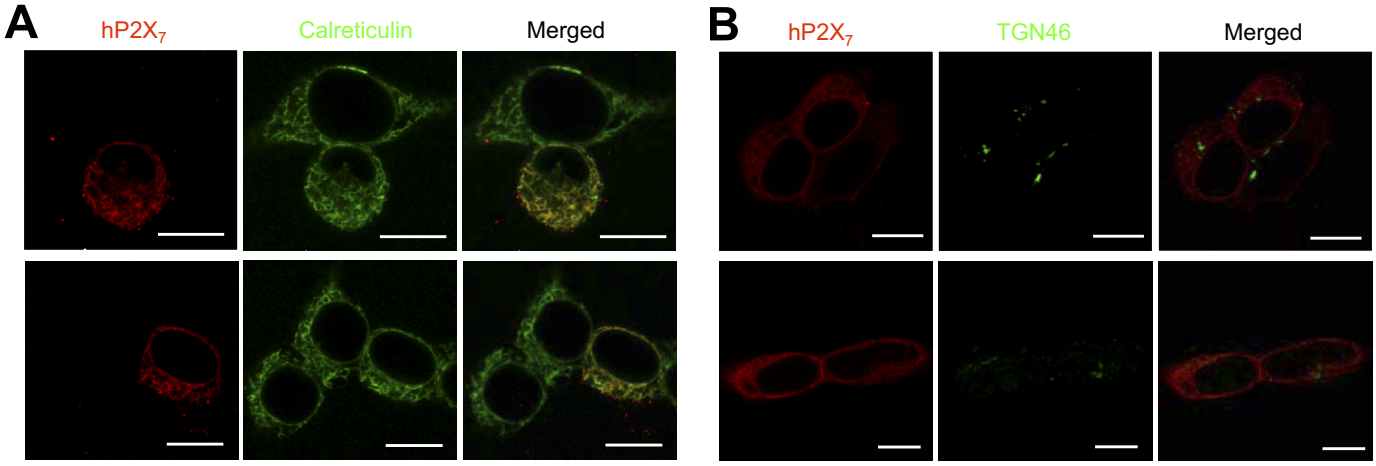

FIGURE 8. **Localization of intracellular hP2X$_7$ proteins within the ER compartment.** Shown are representative immunofluorescence confocal images of double staining for WT hP2X$_7$ proteins (*red*) and calreticulin (*green*), an ER protein marker (*A*), and double staining for WT hP2X$_7$ proteins (*red*) and TGN46 (*green*), a *trans*-Golgi network protein marker (*B*). *Scale bars* = 10 μm.

largely rule out a significant contribution of residue 348 to cell-surface expression and indirectly support a more important role in determining the single-channel properties.

Taken together, our results suggest distinct mechanisms underlying the contribution of residues at positions 155 and 348 to the P2X$_7$ receptor function: an important role for residue 155 in the surface expression and a predominant role for residue 348 in the single-channel function. Further studies are required to better understand these specific roles.

Physiological and Pathological Implications—The expression and function of the P2X$_7$ receptor are vital to its role in mediating the functions of extracellular ATP (see the Introduction). As mentioned above, the H155Y and A348T mutations result from non-synonymous SNPs in the human *P2RX7* gene. A very recent study shows that monocytes from individuals with haplotypes of the hP2X$_7$ receptors carrying A348T exhibit increased ATP-induced secretion of interleukin-1β (78), a pro-inflammatory cytokine that is important in the pathological roles of the P2X$_7$ receptors (13, 14, 80, 81). As demonstrated in our study, the strong difference in hP2X$_7$ receptor function (Fig. 3) depending on which residues at positions 155 and 348 individuals carry is expected to confer differential susceptibilities to diseases. Genetic linkage evidence for disease association of these two non-synonymous SNPs has not yet come forward. However, a previous study reported a trend for linkage of the A348T SNP with the severity of the anxiety disorders (39). Clearly, the results reported and the concepts formulated here should facilitate future genetic linkage studies and therapeutic exploitations (82–84). As far as we are aware, this study provides the first insight into the molecular mechanisms controlling the species difference in the P2X$_7$ receptor functions. Such and other differences in the receptor properties (see the Introduction) may call for cautions to be exercised when the functional roles of the hP2X$_7$ receptor are inferred from studies using laboratory animals.

In conclusion, we have shown that residues at positions 155 and 348 are important in determining the P2X$_7$ receptor function and contribute to the difference in ATP-induced responses

between the human and rat receptors. We have provided evidence suggesting that distinct mechanisms underlie the contribution of these two residues. Such insight into mechanisms controlling the P2X$_7$ receptor functions will help to evolve a better understanding of the important and diverse roles for this receptor in mediating an increasing number of physiological and pathological functions of extracellular ATP.

Acknowledgments—We are grateful to P. Boquet (INSERM452, Nice, France) for the GFP-LAMP1 construct, Drs. C. Cockcroft and R. Karnik for expert assistance in immunostaining, Dr. M. Young (University of Cardiff) for biotin labeling, and Dr. N. Gamper for confocal imaging. We thank Prof. D. J. Beech and Dr. J. Lippiat for constructive discussions during this project.

REFERENCES

1. North, R. A. (2002) *Physiol. Rev.* **82,** 1013–1067
2. Vial, C., Roberts, J. A., and Evans, R. J. (2004) *Trends Pharmacol. Sci.* **25,** 487–493
3. Khakh, B. S., and North, R. A. (2006) *Nature* **442,** 527–532
4. Surprenant, A., and North, R. A. (2009) *Annu. Rev. Physiol.* **71,** 333–359
5. Browne, L. E., Jiang, L. H., and North, R. A. (2010) *Trends Pharmacol. Sci.* **31,** 229–237
6. Solle, M., Labasi, J., Perregaux, D. G., Stam, E., Petrushova, N., Koller, B. H., Griffiths, R. J., and Gabel, C. A. (2001) *J. Biol. Chem.* **276,** 125–132
7. Labasi, J. M., Petrushova, N., Donovan, C., McCurdy, S., Lira, P., Payette, M. M., Brissette, W., Wicks, J. R., Audoly, L., and Gabel, C. A. (2002) *J. Immunol.* **168,** 6436–6445
8. Adinolfi, E., Melchiorri, L., Falzoni, S., Chiozzi, P., Morelli, A., Tieghi, A., Cuneo, A., Castoldi, G., Di Virgilio, F., and Baricordi, O. R. (2002) *Blood* **99,** 706–708
9. Ke, H. Z., Qi, H., Weidema, A. F., Zhang, Q., Panupinthu, N., Crawford, D. T., Grasser, W. A., Paralkar, V. M., Li, M., Audoly, L. P., Gabel, C. A., Jee, W. S., Dixon, S. J., Sims, S. M., and Thompson, D. D. (2003) *Mol. Endocrinol.* **17,** 1356–1367
10. Duan, S., Anderson, C. M., Keung, E. C., Chen, Y., Chen, Y., and Swanson, R. A. (2003) *J. Neurosci.* **23,** 1320–1328
11. Chessell, I. P., Hatcher, J. P., Bountra, C., Michel, A. D., Hughes, J. P., Green, P., Egerton, J., Murfin, M., Richardson, J., Peck, W. L., Grahames, C. B., Casula, M. A., Yiangou, Y., Birch, R., Anand, P., and Buell, G. N. (2005) *Pain* **114,** 386–396
12. Adinolfi, E., Callegari, M. G., Ferrari, D., Bolognesi, C., Minelli, M., Wieckowski, M. R., Pinton, P., Rizzuto, R., and Di Virgilio, F. (2005) *Mol. Biol. Cell* **16,** 3260–3272
13. Matute, C., Torre, I., Pérez-Cerdá, F., Pérez-Samartín, A., Alberdi, E., Etxebarria, E., Arranz, A. M., Ravid, R., Rodríguez-Antigüedad, A., Sánchez-Gómez, M., and Domercq, M. (2007) *J. Neurosci.* **27,** 9525–9533
14. Choi, H. B., Ryu, J. K., Kim, S. U., and McLarnon, J. G. (2007) *J. Neurosci.* **27,** 4957–4968
15. Zhang, X., Chen, Y., Wang, C., and Huang, L. Y. (2007) *Proc. Natl. Acad. Sci. U.S.A.* **104,** 9864–9869
16. Chen, Y., Zhang, X., Wang, C., Li, G., Gu, Y., and Huang, L. Y. (2008) *Proc. Natl. Acad. Sci. U.S.A.* **105,** 16773–16778
17. Nakamoto, T., Brown, D. A., Catalán, M. A., Gonzalez-Begne, M., Romanenko, V. G., and Melvin, J. E. (2009) *J. Biol. Chem.* **284,** 4815–4822
18. Nicke, A. (2008) *Biochem. Biophys. Res. Commun.* **377,** 803–808
19. Surprenant, A., Rassendren, F., Kawashima, E., North, R. A., and Buell, G. (1996) *Science* **272,** 735–738
20. Rassendren, F., Buell, G. N., Virginio, C., Collo, G., North, R. A., and Surprenant, A. (1997) *J. Biol. Chem.* **272,** 5482–5486
21. Chessell, I. P., Simon, J., Hibell, A. D., Michel, A. D., Barnard, E. A., and Humphrey, P. P. (1998) *FEBS Lett.* **439,** 26–30
22. Di Virgilio, F. (2007) *Trends Pharmacol. Sci.* **28,** 465–472
23. Wiley, J. S., Dao-Ung, L. P., Gu, B. J., Sluyter, R., Shemon, A. N., Li, C., Taper, J., Gallo, J., and Manoharan, A. (2002) *Lancet* **359,** 1114–1119
24. Thunberg, U., Tobin, G., Johnson, A., Söderberg, O., Padyukov, L., Hultdin, M., Klareskog, L., Enblad, G., Sundström, C., Roos, G., and Rosenquist, R. (2002) *Lancet* **360,** 1935–1939
25. Zamyatnin, A. A. (1972) *Prog. Biophys. Mol. Biol.* **24,** 107–123
26. Saunders, B. M., Fernando, S. L., Sluyter, R., Britton, W. J., and Wiley, J. S. (2003) *J. Immunol.* **171,** 5442–5446
27. Shemon, A. N., Sluyter, R., Fernando, S. L., Clarke, A. L., Dao-Ung, L. P., Skarratt, K. K., Saunders, B. M., Tan, K. S., Gu, B. J., Fuller, S. J., Britton, W. J., Petrou, S., and Wiley, J. S. (2006) *J. Biol. Chem.* **281,** 2079–2086
28. Sluyter, R., Shemon, A. N., and Wiley, J. S. (2004) *J. Immunol.* **172,** 3399–3405
29. Sluyter, R., Dalitz, J. G., and Wiley, J. S. (2004) *Genes Immun.* **5,** 588–591
30. Glas, R., Sauter, N. S., Schulthess, F. T., Shu, L., Oberholzer, J., and Maedler, K. (2009) *Diabetologia* **52,** 1579–1588
31. Parvathenani, L. K., Tertyshnikova, S., Greco, C. R., Roberts, S. B., Robertson, B., and Posmantur, R. (2003) *J. Biol. Chem.* **278,** 13309–13317
32. McLarnon, J. G., Ryu, J. K., Walker, D. G., and Choi, H. B. (2006) *J. Neuropathol. Exp. Neurol.* **65,** 1090–1097
33. Sanz, J. M., Chiozzi, P., Ferrari, D., Colaianna, M., Idzko, M., Falzoni, S., Fellin, R., Trabace, L., and Di Virgilio, F. (2009) *J. Immunol.* **182,** 4378–4385
34. Díaz-Hernández, M., Díez-Zaera, M., Sánchez-Nogueiro, J., Gómez-Villafuertes, R., Canals, J. M., Alberch, J., Miras-Portugal, M. T., and Lucas, J. J. (2009) *FASEB J.* **23,** 1893–1906
35. Yiangou, Y., Facer, P., Durrenberger, P., Chessell, I. P., Naylor, A., Bountra, C., Banati, R. R., and Anand, P. (2006) *BMC Neurol.* **6,** 12
36. Brough, D., Le Feuvre, R. A., Iwakura, Y., and Rothwell, N. J. (2002) *Mol. Cell. Neurosci.* **19,** 272–280
37. Barden, N., Harvey, M., Gagne, B., Shink, E., Tremblay, M., Raymond, C., Labbe, M., Villeneuve, A., Rochette, D., Bordeleau, L., Stadler, H., Holsboer, F., and Muller-Myhsok, B. (2006) *Am. J. Med. Genet. B Neuropsychiatr. Genet.* **141,** 374–382
38. Lucae, S., Salyakina, D., Barden, N., Harvey, M., Gagné, B., Labbé, M., Binder, E. B., Uhr, M., Paez-Pereda, M., Sillaber, I., Ising, M., Brückl, T., Lieb, R., Holsboer, F., and Müller-Myhsok, B. (2006) *Hum. Mol. Genet.* **15,** 2438–2445
39. Erhardt, A., Lucae, S., Unschuld, P. G., Ising, M., Kern, N., Salyakina, D., Lieb, R., Uhr, M., Binder, E. B., Keck, M. E., Müller-Myhsok, B., and Holsboer, F. (2007) *J. Affect. Disord.* **101,** 159–168
40. Basso, A. M., Bratcher, N. A., Harris, R. R., Jarvis, M. F., Decker, M. W., and Rueter, L. E. (2009) *Behav. Brain Res.* **198,** 83–90
41. Zhou, L., Qi, X., Potashkin, J. A., Abdul-Karim, F. W., and Gorodeski, G. I. (2008) *J. Biol. Chem.* **283,** 28274–28286
42. Solini, A., Cuccato, S., Ferrari, D., Santini, E., Gulinelli, S., Callegari, M. G., Dardano, A., Faviana, P., Madec, S., Di Virgilio, F., and Monzani, F. (2008) *Endocrinology* **149,** 389–396
43. Feng, Y. H., Li, X., Wang, L., Zhou, L., and Gorodeski, G. I. (2006) *J. Biol. Chem.* **281,** 17228–17237
44. Humphreys, B. D., Virginio, C., Surprenant, A., Rice, J., and Dubyak, G. R. (1998) *Mol. Pharmacol.* **54,** 22–32
45. Hibell, A. D., Kidd, E. J., Chessell, I. P., Humphrey, P. P., and Michel, A. D. (2000) *Br. J. Pharmacol.* **130,** 167–173
46. Jiang, L. H., Mackenzie, A. B., North, R. A., and Surprenant, A. (2000) *Mol. Pharmacol.* **58,** 82–88
47. Stokes, L., Jiang, L. H., Alcaraz, L., Bent, J., Bowers, K., Fagura, M., Furber, M., Mortimore, M., Lawson, M., Theaker, J., Laurent, C., Braddock, M., and Surprenant, A. (2006) *Br. J. Pharmacol.* **149,** 880–887
48. Young, M. T., Pelegrin, P., and Surprenant, A. (2007) *Mol. Pharmacol.* **71,** 92–100
49. Sluyter, R., Shemon, A. N., Hughes, W. E., Stevenson, R. O., Georgiou, J. G., Eslick, G. D., Taylor, R. M., and Wiley, J. S. (2007) *Am. J. Physiol. Regul. Integr. Comp. Physiol.* **293,** R2090–R2098
50. Moore, S. F., and Mackenzie, A. B. (2008) *Biochem. Pharmacol.* **76,** 1740–1747
51. Roger, S., Pelegrin, P., and Surprenant, A. (2008) *J. Neurosci.* **28,** 6393–6401
52. Donnelly-Roberts, D. L., Namovic, M. T., Han, P., and Jarvis, M. F. (2009) *Br. J. Pharmacol.* **157,** 1203–1214

53. Roger, S., Mei, Z. Z., Baldwin, J. M., Dong, L., Bradley, H., Baldwin, S. A., Surprenant, A., and Jiang, L. H. (2010) *J. Psychiatr. Res.* **44,** 347–355
54. Liu, X., Ma, W., Surprenant, A., and Jiang, L. H. (2009) *Br. J. Pharmacol.* **156,** 135–142
55. Kim, M., Jiang, L. H., Wilson, H. L., North, R. A., and Surprenant, A. (2001) *EMBO J.* **20,** 6347–6358
56. Kawate, T., Michel, J. C., Birdsong, W. T., and Gouaux, E. (2009) *Nature* **460,** 592–598
57. Davis, I. W., Leaver-Fay, A., Chen, V. B., Block, J. N., Kapral, G. J., Wang, X., Murray, L. W., Arendall, W. B., 3rd, Snoeyink, J., Richardson, J. S., and Richardson, D. C. (2007) *Nucleic Acids Res.* **35,** W375–W383
58. Fiser, A., and Sali, A. (2003) *Bioinformatics* **19,** 2500–2501
59. Fiser, A., and Sali, A. (2003) *Methods Enzymol.* **374,** 461–491
60. Pettersen, E. F., Goddard, T. D., Huang, C. C., Couch, G. S., Greenblatt, D. M., Meng, E. C., and Ferrin, T. E. (2004) *J. Comput. Chem.* **25,** 1605–1612
61. Liu, X., Surprenant, A., Mao, H. J., Roger, S., Xia, R., Bradley, H., and Jiang, L. H. (2008) *Mol. Pharmacol.* **73,** 252–259
62. Mei, Z. Z., Xia, R., Beech, D. J., and Jiang, L. H. (2006) *J. Biol. Chem.* **281,** 38748–38756
63. Xia, R., Mei, Z. Z., Mao, H. J., Yang, W., Dong, L., Bradley, H., Beech, D. J., and Jiang, L. H. (2008) *J. Biol. Chem.* **283,** 27426–27432
64. Sun, C., Chu, J., Singh, S., and Salter, R. D. (2010) *Purinergic Signal.* **6,** 31–45
65. Hille, B. (1992) *Ionic Channels in Excitable Membranes*, 2nd Ed., Sinauer Associates, Inc., Sunderland, MA
66. Jiang, L. H., Rassendren, F., Mackenzie, A., Zhang, Y. H., Surprenant, A., and North, R. A. (2005) *Am. J. Physiol. Cell Physiol.* **289,** C1295–C1302
67. Cabrini, G., Falzoni, S., Forchap, S. L., Pellegatti, P., Balboni, A., Agostini, P., Cuneo, A., Castoldi, G., Baricordi, O. R., and Di Virgilio, F. (2005) *J. Immunol.* **175,** 82–89
68. Wilkinson, W. J., Jiang, L. H., Surprenant, A., and North, R. A. (2006) *Mol. Pharmacol.* **70,** 1159–1163
69. Worthington, R. A., Smart, M. L., Gu, B. J., Williams, D. A., Petrou, S., Wiley, J. S., and Barden, J. A. (2002) *FEBS Lett.* **512,** 43–46
70. Gu, B. J., Zhang, W., Worthington, R. A., Sluyter, R., Dao-Ung, P., Petrou, S., Barden, J. A., and Wiley, J. S. (2001) *J. Biol. Chem.* **276,** 11135–11142
71. Adriouch, S., Dox, C., Welge, V., Seman, M., Koch-Nolte, F., and Haag, F. (2002) *J. Immunol.* **169,** 4108–4112
72. Wiley, J. S., Dao-Ung, L. P., Li, C., Shemon, A. N., Gu, B. J., Smart, M. L., Fuller, S. J., Barden, J. A., Petrou, S., and Sluyter, R. (2003) *J. Biol. Chem.* **278,** 17108–17113
73. Gu, B. J., Sluyter, R., Skarratt, K. K., Shemon, A. N., Dao-Ung, L. P., Fuller, S. J., Barden, J. A., Clarke, A. L., Petrou, S., and Wiley, J. S. (2004) *J. Biol. Chem.* **279,** 31287–31295
74. Le Stunff, H., Auger, R., Kanellopoulos, J., and Raymond, M. N. (2004) *J. Biol. Chem.* **279,** 16918–16926
75. Denlinger, L. C., Sommer, J. A., Parker, K., Gudipaty, L., Fisette, P. L., Watters, J. W., Proctor, R. A., Dubyak, G. R., and Bertics, P. J. (2003) *J. Immunol.* **171,** 1304–1311
76. Adriouch, S., Scheuplein, F., Bähring, R., Seman, M., Boyer, O., Koch-Nolte, F., and Haag, F. (2009) *Purinergic Signal.* **5,** 151–161
77. Young, M. T., Pelegrin, P., and Surprenant, A. (2006) *Br. J. Pharmacol.* **149,** 261–268
78. Stokes, L., Fuller, S. J., Sluyter, R., Skarratt, K. K., Gu, B. J., and Wiley, J. S. (2010) *FASEB J.* **24,** 2916–2927
79. Li, M., Kawate, T., Silberberg, S. D., and Swartz, K. J. (2010) *Nat. Commun.* **1,** 1–7
80. Monif, M., Reid, C. A., Powell, K. L., Smart, M. L., and Williams, D. A. (2009) *J. Neurosci.* **29,** 3781–9391
81. Skaper, S. D., Debetto, P., and Giusti, P. (2010) *FASEB J.* **24,** 337–345
82. Donnelly-Roberts, D. L., and Jarvis, M. F. (2007) *Br. J. Pharmacol.* **151,** 571–579
83. Gorodeski, G. I. (2009) *Expert Opin. Ther. Targets* **13,** 1313–1332
84. Gunosewoyo, H., and Kassiou, M. (2010) *Expert Opin. Ther. Patents* **20,** 625–646